Mott gapping in 3*d* ABO_3 perovskites without Mott-Hubbard interelectronic repulsion energy U

Julien Varignon,[1] Manuel Bibes,[1] and Alex Zunger[2]
[1]*Unité Mixte de Physique, CNRS, Thales, Université Paris Sud, Université Paris-Saclay, 91767, France*
[2]*Energy Institute, University of Colorado, Boulder, Colorado 80309, USA*

(Received 11 October 2018; published 19 July 2019)

The existence of band gaps in Mott insulators such as perovskite oxides with partially filled *3d* shells has been traditionally explained in terms of strong, dynamic interelectronic repulsion codified by the on-site repulsion energy U in the Hubbard Hamiltonian. The success of the "DFT+U approach" where an empirical on-site potential term U is added to the exchange- and correlation density functional theory (DFT) raised questions on whether U in DFT+U represents interelectronic correlation in the same way as it does in the Hubbard Hamiltonian, and if empiricism in selecting U can be avoided. Here we illustrate that *ab initio* DFT *without any* U is able to predict gapping trends and structural symmetry breaking (octahedra rotations, Jahn-Teller modes, bond disproportionation) for all 3*d* ABO_3 perovskites from titanates to nickelates in both spin-ordered and spin-disordered paramagnetic phases. Thus, the mechanism of gap formation due to the Hubbard Hamiltonian dynamic interelectronic correlation is not a requirement in these 3*d* electron compounds. We describe the paramagnetic phases as a supercell where individual sites can have different local environments thereby allowing DFT to develop finite moments on different sites as long as the total cell has zero moment. We use the recently developed strongly constrained appropriately normed exchange and correlation functional (SCAN) that is sanctioned by the usual single-determinant, mean-field DFT paradigm with static correlations, but has a more precise rendering of self-interaction cancelation. Our results suggest that strong dynamic electronic correlations are not playing a universal role in gapping of 3*d* ABO_3 Mott insulators, and opens the way for future applications of DFT for studying a plethora of complexity effects that depend on the existence of gaps, such as doping, defects, and band alignment in ABO_3 oxides.

DOI: 10.1103/PhysRevB.100.035119

I. INTRODUCTION

Transition metal oxide perovskites ABO_3 with a *3d* transition metal atom substituting the *B* site exhibit intriguing metal vs insulator characteristics as well as different forms of magnetism across the series both in their high-temperature (HT) spin-disordered paramagnetic (PM) phases and/or in the low-temperature (LT) spin-ordered phases [1]. Some of the compounds are metallic ($CaVO_3$, $SrVO_3$ or $LaNiO_3$ for instance), while others are insulating, such as titanates $RTiO_3$ (d^1), vanadates RVO_3 (d^2), manganites $CaMnO_3$ (d^3) and $RMnO_3$ (d^4), ferrites $CaFeO_3$ (d^4) and $RFeO_3$ (d^5), cobaltites $RCoO_3$ (d^6), nickelates $RNiO_3$ (d^7) or possibly cuprates $RCuO_3$ (d^8), where *R* is a rare-earth element or yttrium. Concomitantly with the opening of a band gap, one observes a variety of systematic symmetry-breaking modes, such as octahedra deformations in RVO_3 (Ref. [2]) or $RMnO_3$ (Ref. [3] compounds, propagating either in-phase ($Q_2{}^+$ mode) or in antiphase ($Q_2{}^-$ Jahn-Teller), or the *B*-O bond disproportionation B_{oc} observed in the insulating phase of $RNiO_3$ (Ref. [4]) and $CaFeO_3$ (Ref. [5]) (see sketches in Fig. 1). Understanding and controlling such band gaps and the associated lattice distortions and forms of magnetism is central to the ability to dope these oxides, just as is designing specific band offsets in oxide heterojunctions, to the benefit of future oxide electronics. The crucial question here is what minimum theoretical framework is needed to explain and therefore design such gapping-related phenomena.

The standard explanation of gapping in these compounds despite the presence of partially filled *d* shells and the ensuing expected orbital degeneracy is generally formulated in terms of strong interelectronic repulsions appearing in the celebrated Mott-Hubbard model [6–9]. This leads to a uniform explanation of gapping for all *d*-electron ABO_3 compounds and degrees of spin order or disorder, based on the symmetry-conserving interelectronic repulsion, and ensuing localization. Within this framework, the experimental observations of a variety of different symmetry-breaking modes, such as those presented in Fig. 1, or magnetic moments is not related to the gapping mechanism but can appear afterwards as an additional effect.

Whereas density functional theory (DFT) has been shown to be able to address numerous physical effects in such oxides, including ferroelectricity [10], catalysis [11], and electrical battery voltage [12], its use of a single Slater determinant and its mean-field treatment of electron-electron interactions (static correlations) has, according to numerous statements in the literature [13–15], disqualified it for the study of such "strongly correlated" oxides, requiring far more computationally costly dynamically correlated methodologies, such as the dynamical mean field theory (DMFT).

However, the DFT calculations in such demonstrations of failure [13–15] often used a nonspin polarized description and at times exchange correlation functionals that do not distinguish occupied from unoccupied orbitals (local density

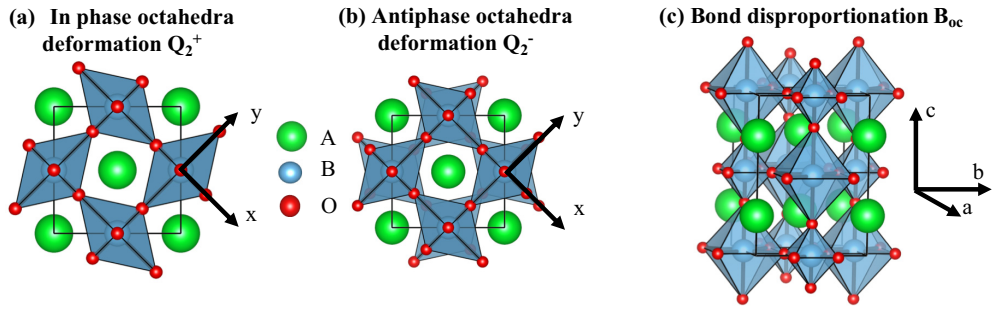

FIG. 1. Sketches of octahedra deformations (a) and (b) and bond disproportionation (c) distortions appearing in some ABO_3 materials.

approximation or generalized gradient approximation functionals without U), and generally neglect sublattice displacements. For example, Ref. [14] demonstrated vanishing band gaps in $LuNiO_3$, in contradiction with experiment, and Ref. [15] demonstrated failure to stabilize the $Q_2{}^+$ octahedra deformation mode in $LaMnO_3$, again, in contradiction with both experiments and DMFT calculations. Such naïve (N-) DFT calculations, however, do not necessarily represent what proper DFT can do, as demonstrated in recent calculations for the binary *3d* oxides MnO, NiO, CoO, and FeO [16] or ABO_3 materials [17–24]. In these calculations [16,24], the PM phase, which is a collection of magnetic moments $\vec{m}$ with random magnitude and direction on each site i but whose sum is zero ($\vec{M} = \sum_i \vec{m}_i = \vec{0}$), was represented by specially constructed supercells that has a total zero spin, but unlike the N-DFT implementations, there was no requirement that each transition metal ion have a zero spin. Such polymorphous representation lowered substantially the total energy relative to the N-DFT representations, while producing finite band gaps and local moments in all studied binary and ternary ABO_3 compounds, in general accord with experiment. The need for an exchange-correlation functional that distinguishes occupied from unoccupied orbitals was satisfied by using a simplified self-interaction corrected functional in the form of "DFT+U" [25]. The use of "U" created sometimes the false impression that this approach owes its success in explaining gaps to the interelectronic repulsion and localization, just as in the Mott-Hubbard view.

To examine if the explanation of Mott-Hubbard gapping mandates an explicit Hubbard U, we have performed DFT calculations without U, using the strongly constrained appropriately normed SCAN [26] DFT functional, that better cancels the self-interaction error, thus creating more compact orbitals. The use of the SCAN functional for transition metals and transition metal oxides is reported in many papers [27–32]. Unlike these publications we do not just study how the SCAN functional behaves with ternary oxides on gaps, structural features or electron localization, but we tackle a different problem: is the Mott-Hubbard model required to capture trends in gapping, structural motions or magnetic moments in ABO_3 materials? Here we show that (i) DFT, without any U parameter but with an exchange-correlation functional better representing self-interaction errors, is sufficient to explain trends in properties of ternary ABO_3 oxides in both LT spin-ordered and HT PM phases; (ii) since DFT-no-U and its static mean-field treatment of electron interactions are largely sufficient to produce Mott insulation, ABO_3 oxide perovskites may certainly be complicated but they are not necessarily strongly dynamically correlated and (iii) thus, Mott gapping in such specific cases may not sweepingly obey the celebrated Mott-Hubbard explanation of formation of two electron sites that depends on the existence of *d*-like band edges and on interelectronic repulsion exceeding band width, neither of which are needed in the current explanation. However, our results do not imply that if DFT works for a material, then all forms of correlations do not play a role.

II. METHOD

We have performed DFT [33,34] total energy minimization with respect to lattice parameters and cell-internal atomic positions of different perovskite oxides with *d* fillings from 1 to 8 electrons. Structure types compared for their total energy included orthorhombic (*Pbnm*), monoclinic ($P2_1/b$ and $P2_1/n$) and rhombohedral (*R-3c*), whereas spin configurations examined included FM, as well as classical *A*, *C*, and *G*-type antiferromagnetic (AFM) orders, and more complex *S*-type AFM order based on $\uparrow\uparrow\downarrow\downarrow$ spins chains in the (*ab*) plane with different stackings along the *c* axis. We emphasize here that we did not explore the relative stability of the different magnetic orders and we just focused on the spin order experimentally observed at low temperature for each compound. The paramagnetic (PM) spin-disordered state has been modeled using the special quasirandom structures (SQS) method [35], following Refs. [16] and [24], which represents a random "alloy" of up and down (collinear) spins with total spin zero, within the $2 \times 2 \times 2$ orthorhombic or monoclinic cells (32 ABO_3 formula units containing 160 atoms). Convergence with SQS supercell size was tested and found adequate at 160 atoms [24]. All atomic displacements as well as breaking of degeneracies of partially occupied e_g and t_{2g} levels are allowed as long as they reduce the total energy. Amplitudes of the energy-minimizing distortions were determined by performing a symmetry adapted mode analysis [36,37] with a reference structure set to the ideal high symmetry cubic *Pm-3m* structure of perovskites. The lattice parameter of this hypothetical cubic structure is fixed to the ground state pseudocubic lattice parameter.

III. RESULTS

Calculated structural and electronic properties. Figure 2 summarizes the calculated band gap ΔE (in eV), magnetic

	d filling	Sym.	Mag.	ΔE_{NM} (mev/f u)	Electronic properties		Structural distortions		
					E_g (eV)	M_{3d} (μ_B)	Q_2^+ (Å)	Q_2^- (Å)	B_{oc} (Å)
$YTiO_3$	$t_{2g}^1e_g^0$	*Pbnm*	FM	-242	0.08	0.92 (0.84[a])	0.03	-	-
		Pbnm	PM	-218	0.33 (1.20[b])	0.84	0.02 (0.00[c])	-	-
$LaTiO_3$	$t_{2g}^1e_g^0$	*Pbnm*	AFMG	-75	0.05	0.67 (0.46[d])	0.06	-	-
		Pbnm	PM	-84	0.14 (0.20[b])	0.78	0.04 (0.04[c])	-	-
YVO_3	$t_{2g}^2e_g^0$	*Pbnm*	AFMG	-1052	0.89	1.77 (1.72[e])	0.19 (0.14[e])	-	-
		P-1	PM	-978	0.55 (1.60[f])	1.82	NA	NA	-
$LaVO_3$	$t_{2g}^2e_g^0$	*Pbnm*	AFMC	-864	0.78	1.78 (1.30[g])	0.00 (0.01[h])	0.09 (0.08[h])	-
		P-1	PM	-833	0.36 (1.10[i])	1.80	NA	NA	-
$CaMnO_3$	$t_{2g}^3e_g^0$	*Pbnm*	AFMG	-2049	0.79	2.62 (2.64[j])	0.01	-	-
		Pbnm	PM	-2036	1.46 (ins.)	2.62	0.01 (0.04[k])	-	-
$LaMnO_3$	$t_{2g}^3e_g^1$	*Pbnm*	AFMA	-1783	0.52	3.65 (3.70[l])	0.28	-	-
		Pbnm	PM	-1758	0.30 (0.24[m]-1.70[n])	3.60	0.32 (0.30[o])	-	-
$CaFeO_3$	$t_{2g}^3e_g^0 + t_{2g}^3e_g^2$	$P2_1$	AFMS	-1474	0.20	2.72-3.67 (2.48-3.48[p])	0.00	-	0.13
		$P2_1/n$	PM	-1449	0.07 (0.25[q])	2.66-3.72	0.00 (0.04[p])	-	0.14 (0.18[p])
$LaFeO_3$	$t_{2g}^3e_g^2$	*Pbnm*	AFMG	-1073	1.67 (2.10[i])	3.94 (4.60[r])	0.01	-	-
		Pbnm	PM	-936	0.52	4.04	0.01 (0.00[s])	-	-
$YCoO_3$	$t_{2g}^6e_g^0$	*Pbnm*	NM	-	1.48 (ins.[t])	-	0.06 (0.05[t])	-	-
$YNiO_3$	$t_{2g}^6e_g^2 + t_{2g}^6e_g^0$	$P2_1/n$	AFMS	-353	0.92	1.41-0.00 (1.70-0.40[u])	0.05	-	0.18
		$P2_1/n$	PM	-350	0.59 (0.20[i]-1.00[v])	1.38-0.28	0.05 (0.05[w])	-	0.17 (0.13[w])
$LaCuO_3$	$t_{2g}^6e_g^2$	*R-3c*	AFMG	-143	0.48 (?)	0.70 (?)	-	-	-

FIG. 2. Key properties of oxide perovskites with the SCAN meta-GGA functional without U. We use the SQS supercell for the PM phase. ΔE_{NM} (meV/f u) is the energy difference between the current spin polarized and the Naive DFT (N-DFT) solution. E_g is the band gap (in eV), M_{3d} is the local moment (in μ_B) associated with the *B* cation. Q_2^-, Q_2^+ and B_{oc} are the octahedral deformation amplitudes (in Å) (experimental values are provided in parenthesis). Ins. stands for insulating phases. Experimental values are taken from a: Ref. [40], b: Ref. [41], c: Ref. [42], d: Ref. [43], e: Ref. [44], f: Ref. [45]; g: Ref. [46], h: Ref. [47], i: Ref. [48], j: Ref. [49], k: Ref. [50], l: Ref. [51], m: Ref. [52], n: Ref. [53], o: Ref. [54], p: Ref. [5], q: Ref. [55], r: Ref. [56], s: Ref. [57], t: Ref. [58], u: Ref. [4], v: Ref. [59], w: Ref. [60].

moment M_{3d} (in μ_B) associated with the *B* cations and amplitudes of distortions (in Å) associated with $Q_2{}^+$, $Q_2{}^-$ and bond disproportionation motions, all done without Hubbard U, compared with experimental values available in literature. The calculated energy-minimizing lattice type agrees with experiments with the exception of YVO_3 and $LaVO_3$ in the PM phase and $CaFeO_3$ in the AFM phase. In the two vanadates, the strongly entangled spin and orbital degrees of freedom induce small lattice distortions on each octahedra in the PM phase (where each transition metal element experiences a unique potential), thus reducing the symmetry from $P2_1/c$ to *P*-1 [38]. However, the lattice parameters, *B*-O-*B* angles and *B*-O bond lengths are very similar to the respective quantities observed in experimental structures. For $CaFeO_3$, the AFM-*S* magnetic order that we have used to approximate the experimentally observed AFM spiral [5] breaks the inversion center and induces some small lattice distortions such as polar displacements [39], thus producing a polar $P2_1$ space group instead of a centrosymmetric $P2_1/n$ symmetry.

Band gaps without U. All ABO_3 compounds tested here are insulators in both their spin-ordered and spin-disordered PM solutions (Fig. 2). These results agree with the insulating character observed experimentally (some experimental values available in literature are reported in Fig. 2) and also reproduce trends observed with DFT+U and DMFT simulations on some of these materials (e.g.,$R$$TiO_3$, RVO_3, $RMnO_3$ and $RNiO_3$, see references therein). For instance, we observe insulation in the yttrium nickelate $YNiO_3$ compound in both AFM and PM phases, as DMFT does in the $LuNiO_3$ PM phase [14,61]. Likewise, we also observe an increase in the band gap when going from rare-earth titanates (d^1) to rare-earth vanadates (d^2) in agreement with experimental observations [41,45]. We emphasize here that experimental data of structural and electronic properties on bulk and stoichiometric $LaCuO_3$ crystals are scarce and diverging hindering confirmation of the SCAN-DFT calculation. Finally, just as standard exchange and correlation functionals underestimate the band gap of the highly uncorrelated semiconductors such as Si and GaAs, the SCAN functional behaves similarly for ABO_3 materials and one may improve the band gap description and related quantities by using GW corrections [62].

Magnetic moments. Our calculations provide magnetic moment values that are comparable to experimental quantities available in literature (see Fig. 2). For instance, we capture the decrease of the magnetic moment of Ti cations when going from $YTiO_3$ to $LaTiO_3$ [40,43]. Due to the presence of a double local environment (DLE) for Ni and Fe cations in $YNiO_3$ and $CaFeO_3$, respectively, two very different magnetic moments are extracted from our simulations. These quantities, compatible with experimental values, point towards a disproportionation of the unstable 3+ and 4+ formal oxidation states (FOS) of Ni and Fe cations, respectively, towards their more stable 2+/4+ and 3+/5+ FOS.

Trends in energy differences between different phases. The energy gain in forming local moments is given by the total energy difference E_{NM}-E_{AFM}. As the number of unpaired 3*d* electrons increases, we see that this energy strongly increases, signaling the large energy gain obtained by forming local

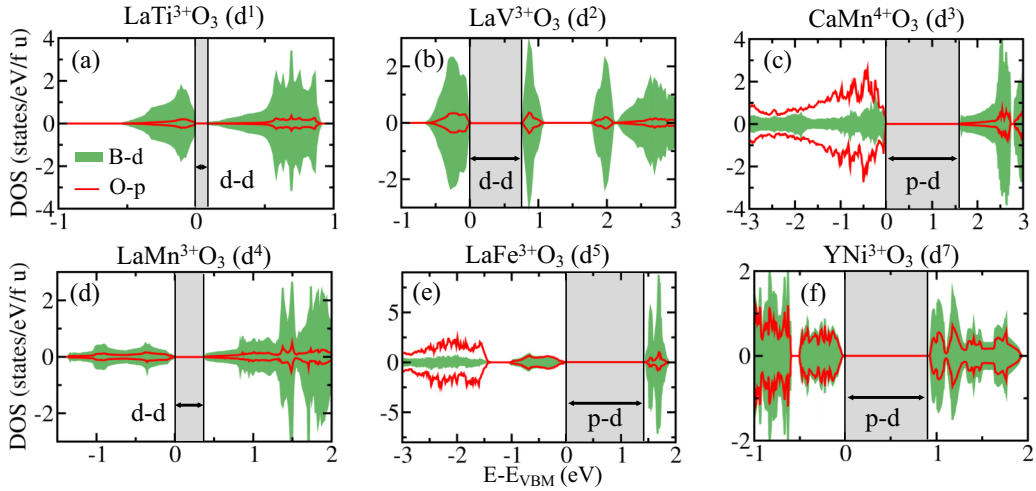

FIG. 3. Projected density of states (in states/eV/f. u) on *B*-*d* levels (filled green) and O-*p* levels (red line) averaged on all sites in the low temperature phase. Band edges are shown with the vertical lines. The band gap is represented by the light grey area.

magnetic moments, and thus the irrelevance of the NM ansatz (Fig. 2). The energy cost for forming a random configuration from an ordered one is (E_{PM}-E_{AFM})-TS where the first term is the contribution of the internal $T = 0$ energy. For all compounds studied (E_{PM}-E_{AFM}) > 0, i.e., the spin-ordered states are just slightly more stable than the PM solution. The entropy contribution will cause an order -disorder transition at finite $T_{Néel}$. $LaTiO_3$ is an exception in which (E_{PM}-E_{AFM}) < 0, i.e., the experimentally observed AFM-*G* state is higher in energy than the PM state. This delicate balance could be because other magnetic configurations occur at low T. We checked the FM spin order (in the spirit of $YTiO_3$) for this compound and found that the FM order now represents an energy gain of 10 meV/f.u over the PM phase. Interestingly $LaTiO_3$ in the FM spin order is still an insulator ($E_g = 0.02$ eV) with similar distortions to the PM and AFM-*G* solutions. It is possible that an exhaustive search for other spin configurations will change the result somewhat. Indeed, we did not perform such an exhaustive search.

Electronic Localization without U. It is interesting to analyze the electronic localization of the d electrons in those perovskite oxides that are believed to be strongly dynamically correlated systems (d^1, d^2, d^4, and d^7 materials, for instance). We report in Fig. 4 the electronic charge density at the top of the valence band in the low temperature spin-ordered phase of $LaTiO_3$ (d^1), YVO_3 (d^2), $LaMnO_3$ (d^4), and $YNiO_3$ (d^7). In agreement with the pDOS reported in Fig. 3, one notices increasing density on the O atoms when going from light to heavier transition metal atoms, underlining the progressive shift from "Mott insulators" ($LaTiO_3$, YVO_3, Figs. 4(a) and 4(b) to "charge transfer insulator" [$YNiO_3$, Fig. 4(d)] behaviors. In $LaTiO_3$ [Fig. 4(a)], the single Ti^{3+} d electron is localized in a linear combination of the three t_{2g} levels, whose relative coefficients are alternating on neighboring Ti sites. In YVO_3 [Fig. 4(b)], the additional d electron sits in a combination of the d_{xy} and d_{xz} or d_{yz} orbital, with alternating coefficients on neighboring sites due to the presence of the Q_2^+ motions in the low-temperature phase (see Fig. 2). We observe a similar situation in $LaMnO_3$ [Fig. 4(c)]: the Mn^{3+} e_g electron is localized either in d_{x^2} or d_{y^2} orbitals between neighboring Mn sites in the (*ab*) plane but with similar stackings along the c axis. Finally, a "charge ordered" picture is observed in $YNiO_3$ [Fig. 4(d)] with Ni cations sitting in an extended (compressed) octahedra bearing approximately 2 (0) electrons on the e_g levels. This is clearly proving a charge disproportionated insulating state with Ni ions adopting their more stable 2+ and 4+ FOS instead of the unstable 3+ FOS. Similar observations were obtained for other members such as $YTiO_3$, $LaVO_3$ or $CaFeO_3$, independently of the spin-order/disorder.

How displacements affect or create gapping. To understand the role of Q_2 octahedra deformations and bond disproportionation motion on the gap opening, we use as a starting

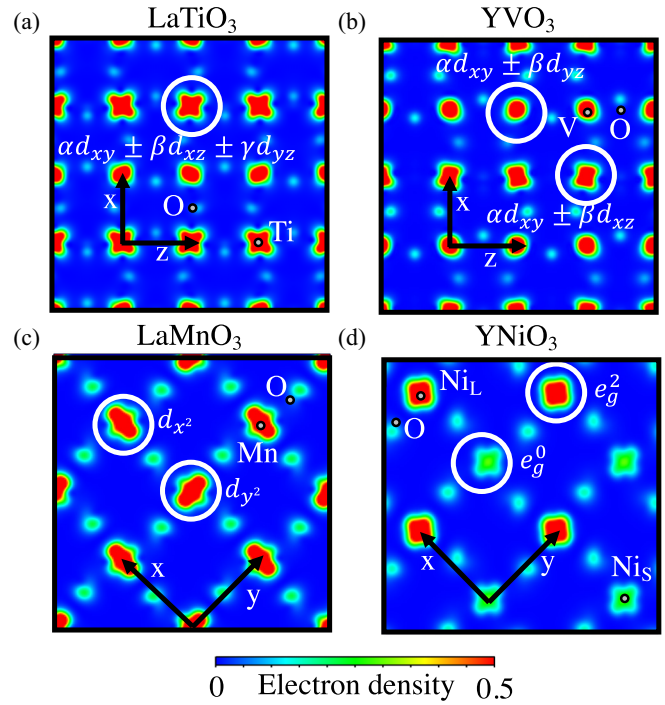

FIG. 4. Partial charge density maps of levels at the top of the valence band in some selected "correlated oxide perovskites".

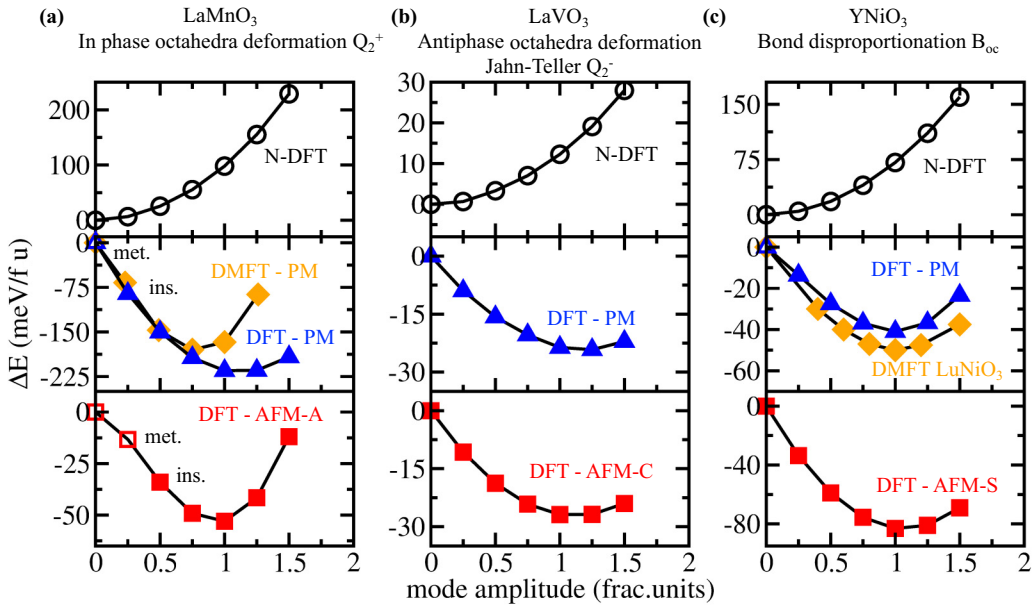

FIG. 5. Energy gains ΔE (in meV/f.u with respect to the 0-mode amplitude) associated with Q_2 distortions (a) and (b) and the bond disproportionation (c) modes (in fractional units) obtained by the naïve nonmagnetic N-DFT (black circles, upper panel), the PM modelled with a SQS supercell (blue triangles, middle panel), and the AFM order (red squares, lower panel). The DMFT potential (orange diamonds) for the PM phase of $LaMnO_3$ and $LuNiO_3$ extrapolated from Refs. [15,61] are also reported. Filled and unfilled symbols correspond to insulating (ins.) and metallic (met.) solutions. The reference structure at 0 amplitude of Q_2 or B_{oc} modes is set to a material displaying octahedra rotations and antipolar motions of ions. A fractional unit equals to 1 corresponds to amplitude appearing in the ground state AFM structure.

configuration a high symmetry *Pm-3m* phase and then apply to it successively all displacement modes appearing in the ground state AFM structure (i.e., O_6 rotations, antipolar displacements of ions). We then freeze the Q_2 or B_{oc} modes and compute the potential energy surface vs amplitude of the modes for NM, AFM, and PM solutions in $LaMnO_3$ (Q_2^+ mode), $LaVO_3$ (Q_2^- mode), and $YNiO_3$ (B_{oc} mode). This protocol has been used in Ref. [15] to demonstrate the inability of naïve N-DFT to stabilize Q_2^+ motions in $LaMnO_3$ and the crucial role of strong dynamic correlation to obtain such displacements. Our results for the same NM ansatz are reported in Fig. 5, where we confirm that this naïve model yields a single well potential whose energy minimum is located in zero amplitude, i.e., these structural distortions do not appear. Comparing with the full DFT calculation in Fig. 5 clearly shows, however, that N-DFT is not what DFT can actually do, the latter producing distortions where they appear experimentally. Moving to AFM and PM spin-polarized solutions, we observe that the energy minimum of the different potentials is located at nonzero amplitude of Q_2 and B_{oc} modes. We conclude that DFT without an interelectronic U can stabilize these previously believed to be "correlation-induced lattice distortions" [14,15] if minimal ingredients are provided to the simulations. It is evident that dynamic correlation effects are not forcing these distortions whose role was previously hampered by a false initial hypothesis.

The role of atomic displacements on the gap opening. Opened and closed symbols in Fig. 5 denote metallic or insulating solutions, respectively. Upon increasing the amplitude of the Q_2^+ and B_{oc} modes in $LaMnO_3$ and $YNiO_3$, respectively, a band gap opens in the PM and AFM solutions. $LaVO_3$ is different where rotations plus antipolar displacements of ions are sufficient to produce an insulating state since the Q_2^- Jahn-Teller (JT) mode is not important for the gap opening. The present SCAN-no-U results are consistent with DFT+U and DMFT simulations in $LaMnO_3$ [13,23,24,63] and RVO_3 [18,24,64], as well as the experimental observation of insulating states in RVO_3 irrespective of the presence of the JT Q_2^- mode [65]. Surprisingly, even without any amplitude of the disproportionation B_{oc} mode, $YNiO_3$ already exhibits a clear-cut view of the Ni electronic structures with one Ni site bearing a magnetic moment of 1.06 (1.26) μ_B and the other one a value around 0.72 (0.00) μ_B in the PM (AFM) solution [Fig. 5(c)]. It follows that $YNiO_3$ has a spontaneous tendency to undergo disproportionation effects through an electronic instability transforming the unstable 3+ FOS of Ni cations to the more stable 2+ and 4+ FOS in the insulating phase. Nevertheless, only the AFM order can render an insulating state without bond disproportionation B_{oc} mode [Fig. 5(c)]; this is consistent with the fact that the PM phase of $YNiO_3$ without bond disproportionation is found to be metallic in experiments [4]. The observation of an electronic instability agrees with our recent DFT+U study [24] and with numerous DMFT calculations identifying a spontaneous tendency of Ni^{3+} cations to undergo disproportionation effects [61,66].

IV. DISCUSSION

So far, we have shown the ability of the SCAN functional to capture the formation of basic physical quantities (e.g., band gap, magnetic moments, structural motions) of ABO_3 materials upon various *d* fillings. We may now question the ability of this functional to reproduce physical trends within series showing isoelectronic configurations.

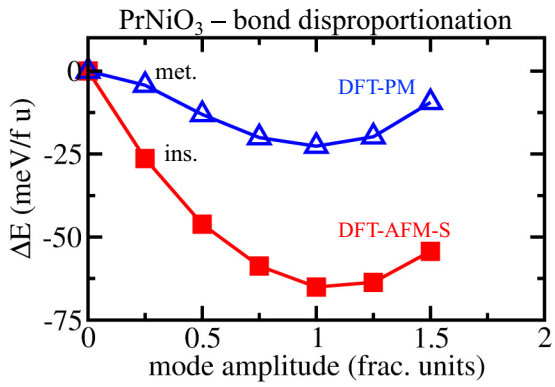

FIG. 6. Properties of isoelectronic compounds. Energy difference as a function of the bond disproportionation (in fractional units) in $PrNiO_3$ in the AFM (squares) and PM (triangles) magnetic orders. Filled and unfilled symbols correspond to insulating and metallic solutions, respectively. The reference structure at 0 amplitude of the B_{oc} mode is set to a material displaying octahedra rotations and antipolar motions of ions. A fractional unit equal to 1 corresponds to the amplitude appearing in the ground state structure.

The dependence of the octahedra deformations on the existence of the local magnetic moments: The case of $SrVO_3$. For instance, $SrVO_3$ (d^1) displays a paramagnetic metallic state at all temperatures, while the isolectronic rare-earth titanates $RTiO_3$ exhibit insulating states. We have explored the paramagnetic state of $SrVO_3$ using the constrained magnetic approach proposed by Franchini *et al.* [67,68] (we restricted V^{4+} spins to be aligned along z, since spins have the tendency to flip during the self-consistent field). Unlike the isoelectronic $RTiO_3$ compounds, $SrVO_3$ relaxes to a cubic metallic phase, thus showing no octahedra deformations. This can be explained using the 1926 Goldschmidt tolerance factor close to 1, which implies cubic stability in agreement with experiments. In contrast, we have shown that isovalent $YTiO_3$ and $LaTiO_3$ are insulating for both paramagnetic and spin-ordered phases.

The case of $PrNiO_3$. The $RNiO_3$ compounds form another important family of ABO_3 perovskites in which materials with an A site cation presenting a small ionic radius are insulating in both AFM and PM phases (R = Lu-Sm, Y), while the remaining compounds (R = Nd, Pr) are only insulators in the AFM phase [69]. We correctly find that the geometry relaxation for $PrNiO_3$ with the AFM order results in an insulating monoclinic cell showing a band gap of 0.78 eV and disproportionation effects ($Q_{Boc} = 0.15$ Å, $\mu_{NiL} = 1.38\,\mu_B$, and $\mu_{NiS} = 0\,\mu_B$), whose amplitudes are reduced with respect to $YNiO_3$. Just as in the case of $YNiO_3$, the stabilization of the breathing mode is not essential for the gap opening and the AFM order is already sufficient to produce a sizable band gap of 0.56 eV and an asymmetry of magnetic moments ($\mu_{NiL} = 1.21\,\mu_B$ and $\mu_{NiS} = 0\,\mu_B$) (see the energy potential surface as a function of B_{oc} amplitude when starting from a cell with only rotations and antipolar displacement presented in Fig. 6). Using the AFM structure but with a PM order, $PrNiO_3$ is also willing to adopt a disproportionated cell whose amplitude is a priori not enough to produce insulation (Fig. 6). In contrast to the AFM order and $YNiO_3$, the PM solution without bond disproportionation does not show any asymmetry of magnetic moments, all Ni cations bear a spin of 0.93 μ_B. This observation signals the absence of a spontaneous electronic instability toward a disproportionation in the PM cell for $PrNiO_3$, in agreement with experiments. Nevertheless, a full structural relaxation with the PM order yields an insulating disproportionated cell at 0 K for $PrNiO_3$ with a narrow band gap of 0.30 eV in contrast with experiments, i.e., it becomes an insulator at the AFM transition ($T_N = 135$ K [69]). This discrepancy could result from an exaggerated electron localization in SCAN that contributes to (i) bond disproportionation and (ii) Ni magnetic moments substantially larger in SCAN-no-U ($Q_{Boc} = 0.17$ and 0.15 Å, $\mu_{NiL} = 1.41$ and $1.35\,\mu_B$ for R = Y and Pr, respectively) than in the GGA+U calculations ($Q_{Boc} = 0.14$ and 0.11 Å, $\mu_{NiL} = 1.26$ and $1.17\,\mu_B$ for R = Y and Pr, respectively) of Refs. [20,24]. Overestimated magnetic moments are not specific to ABO_3 materials and instead seem inherent to the SCAN functional [27,70], which will have to be improved in this respect.

V. CONCLUSION

We have shown that a DFT using a functional without on-site correlation energy U but with better amending self-interaction errors captures the basic properties of 3*d* electron transition metal oxide perovskites namely band gap, magnetic moments, relative *B*-*d* to *O*-p levels positions and all structural features, by using a polymorphous representation allowing energy lowering formation of (i) magnetic moments, (ii) atomic displacements and octahedral rotations, and (iii) breaking of crystal field symmetry of partially occupied orbitals. We further show that lattice distortions including the Jahn-Teller and bond disproportionation modes, are captured by single-determinant, mean field DFT without U parameter suggesting that dynamic correlations are not the universal controlling factor here. Success of DFT for a given case does not exclude the existence of other forms of correlation. Furthermore, the success of DFT does not imply that Coulomb interactions are not important, because DFT certainly includes (mean-field like Hartree) Coulomb interaction. However, this is very different than the highly complex treatment of the non-mean-field Hubbard-like U interaction term in the Hubbard Hamiltonian. The latter effect is excluded in the much simpler present calculation, which still provides good and material-specific results.

ACKNOWLEDGMENTS

This work received support from the European Research Council (ERC) Consolidator grant MINT under the Contract No. 615759. Calculations took advantages of the Occigen machines through the DARI project EPOC A0020910084 and of the DECI resource FIONN in Ireland at ICHEC through the PRACE project FiPSCO. The work of A.Z. was supported by Department of Energy, Office of Science, Basic Energy Science, MSE division under Grant No. DE-FG02-13ER46959 to CU Boulder. J.V. acknowledges technical support from A. Ralph at ICHEC supercomputers.

[1] D. I. Khomskii, *Transition Metal Compounds* (Cambridge University Press, Cambridge, 2014).
[2] S. Miyasaka, Y. Okimoto, M. Iwama, and Y. Tokura, Phys. Rev. B **68**, 100406(R) (2003).
[3] X. Qiu, T. Proffen, J. F. Mitchell, and S. J. L. Billinge, Phys. Rev. Lett. **94**, 177203 (2005).
[4] J. A. Alonso, J. L. García-Muñoz, M. T. Fernández-Díaz, M. A. G. Aranda, M. J. Martínez-Lope, and M. T. Casais, Phys. Rev. Lett. **82**, 3871 (1999).
[5] P. M. Woodward, D. E. Cox, E. Moshopoulou, A. W. Sleight, and S. Morimoto, Phys. Rev. B **62**, 844 (2000).
[6] N. F. Mott and Z. Zinamon, Rep. Prog. Phys. **33**, 881 (1970).
[7] N. Mott, *Metal-Insulator Transitions* (CRC Press, Boca Raton, FL, 1990).
[8] J. Hubbard, Proc. R. Soc. A Math. Phys. Eng. Sci. **276**, 238 (1963).
[9] J. Hubbard, Proc. R. Soc. London Ser. A **281**, 401 (1964).
[10] R. E. Cohen, Nature (London) **358**, 136 (1992).
[11] G. Pacchioni, J. Chem. Phys. **128**, 182505 (2008).
[12] F. Lin, I. M. Markus, D. Nordlund, T.-C. Weng, M. D. Asta, H. L. Xin, and M. M. Doeff, Nat. Commun. **5**, 3529 (2014).
[13] E. Pavarini and E. Koch, Phys. Rev. Lett. **104**, 086402 (2010).
[14] H. Park, A. J. Millis, and C. A. Marianetti, Phys. Rev. Lett. **109**, 156402 (2012).
[15] I. Leonov, D. Korotin, N. Binggeli, V. I. Anisimov, and D. Vollhardt, Phys. Rev. B **81**, 075109 (2010).
[16] G. Trimarchi, Z. Wang, and A. Zunger, Phys. Rev. B **97**, 035107 (2018).
[17] J. Varignon, M. N. Grisolia, D. Preziosi, P. Ghosez, and M. Bibes, Phys. Rev. B **96**, 235106 (2017).
[18] J. Varignon, N. C. Bristowe, E. Bousquet, and P. Ghosez, Sci. Rep. **5**, 15364 (2015).
[19] N. C. Bristowe, J. Varignon, D. Fontaine, E. Bousquet, and P. Ghosez, Nat. Commun. **6**, 6677 (2015).
[20] J. Varignon, M. N. Grisolia, J. Íñiguez, A. Barthélémy, and M. Bibes, Npj Quantum Mater. **2**, 21 (2017).
[21] A. Mercy, J. Bieder, J. Íñiguez, and P. Ghosez, Nat. Commun. **8**, 1677 (2017).
[22] Y. Zhang, M. M. Schmitt, A. Mercy, J. Wang, and P. Ghosez, Phys. Rev. B **98**, 081108(R) (2018).
[23] T. A. Mellan, F. Cora, R. Grau-Crespo, and S. Ismail-Beigi, Phys. Rev. B **92**, 085151 (2015).
[24] J. Varignon, M. Bibes, and A. Zunger, Nat. Commun. **10**, 1658 (2019).
[25] S. L. Dudarev, G. A. Botton, S. Y. Savrasov, C. J. Humphreys, and A. P. Sutton, Phys. Rev. B **57**, 1505 (1998).
[26] J. Sun, A. Ruzsinszky, and J. P. Perdew, Phys. Rev. Lett. **115**, 036402 (2015).
[27] Y. Fu and D. J. Singh, Phys. Rev. Lett. **121**, 207201 (2018).
[28] G. Sai Gautam and E. A. Carter, Phys. Rev. Mater. **2**, 095401 (2018).
[29] H. Peng and J. P. Perdew, Phys. Rev. B **96**, 100101(R) (2017).
[30] Y. Zhang, D. A. Kitchaev, J. Yang, T. Chen, S. T. Dacek, R. A. Sarmiento-Pérez, M. A. L. Marques, H. Peng, G. Ceder, J. P. Perdew, and J. Sun, Npj Comput. Mater. **4**, 9 (2018).
[31] A. Chakraborty, M. Dixit, D. Aurbach, and D. T. Major, Npj Comput. Mater. **4**, 60 (2018).
[32] J. W. Furness, Y. Zhang, C. Lane, I. G. Buda, B. Barbiellini, R. S. Markiewicz, A. Bansil, and J. Sun, Commun. Phys. **1**, 11 (2018).
[33] G. Kresse and J. Hafner, Phys. Rev. B **47**, 558 (1993).
[34] G. Kresse and J. Furthmüller, Comput. Mater. Sci. **6**, 15 (1996).
[35] A. Zunger, S.-H. Wei, L. G. Ferreira, and J. E. Bernard, Phys. Rev. Lett. **65**, 353 (1990).
[36] D. Orobengoa, C. Capillas, I. Aroyo, and J. M. Perez, J. Appl. Crystallogr. **42**, 820 (2009).
[37] J. M. Perez-Mato, D. Orobengoa, and M. I. Aroyo, Acta Crystallogr. A **66**, 558 (2010).
[38] K. I. Kugel and D. I. Khomskii, Sov. Phys.-JETP **37**, 725 (1973).
[39] G. Giovannetti, S. Kumar, D. Khomskii, S. Picozzi, and J. van den Brink, Phys. Rev. Lett. **103**, 156401 (2009).
[40] J. D. Garrett, J. E. Greedan, and David A. MacLean, Mater. Res. Bull. **16**, 145 (1981).
[41] Y. Okimoto, T. Katsufuji, Y. Okada, T. Arima, and Y. Tokura, Phys. Rev. B **51**, 9581 (1995).
[42] A. C. Komarek, H. Roth, M. Cwik, W.-D. Stein, J. Baier, M. Kriener, F. Bourée, T. Lorenz, and M. Braden, Phys. Rev. B **75**, 224402 (2007).
[43] M. Cwik, T. Lorenz, J. Baier, R. Müller, G. André, F. Bourée, F. Lichtenberg, A. Freimuth, R. Schmitz, E. Müller-Hartmann, and M. Braden, Phys. Rev. B **68**, 060401(R) (2003).
[44] M. Reehuis, C. Ulrich, P. Pattison, B. Ouladdiaf, M. C. Rheinstädter, M. Ohl, L. P. Regnault, M. Miyasaka, Y. Tokura, and B. Keimer, Phys. Rev. B **73**, 094440 (2006).
[45] A. A. Tsvetkov, F. P. Mena, P. H. M. Van Loosdrecht, D. van der Marel, Y. Ren, A. A. Nugroho, A. A. Menovsky, I. S. Elfimov, and G. A. Sawatzky, Phys. Rev. B **69**, 075110 (2004).
[46] V. G. Zubkov, G. V. Bazuev, V. A. Perelyaev, and G. P. Shveikin, Sov. Phys. Solid State **15**, 107 (1973).
[47] P. Bordet, C. Chaillout, M. Marezio, Q. Huang, A. Santoro, S. W. Cheong, H. Takagi, C. S. Oglesby, and B. Batlogg, J. Solid State Chem. **106**, 253 (1993).
[48] T. Arima, Y. Tokura, and J. B. Torrance, Phys. Rev. B **48**, 17006 (1993).
[49] Neetika, A. Das, I. Dhiman, A. K. Nigam, A. K. Yadav, D. Bhattacharyya, and S. S. Meena, J. Appl. Phys. **112**, 123913 (2012).
[50] W. Paszkowicz, J. Piętosa, S. M. Woodley, P. A. Dłużewski, M. Kozłowski, and C. Martin, Powder Diffr. **25**, 46 (2010).
[51] J. B. A. A. Elemans, B. Van Laar, K. R. Van Der Veen, and B. O. Loopstra, J. Solid State Chem. **3**, 238 (1971).
[52] R. Mahendiran, S. K. Tiwary, A. K. Raychaudhuri, R. Mahesh, and C. N. R. Rao, Phys. Rev. B **54**, R9604(R) (1996).
[53] T. Saitoh, A. E. Bocquet, T. Mizokawa, H. Namatame, A. Fujimori, M. Abbate, Y. Takeda, and M. Takano, Phys. Rev. B **51**, 13942 (1995).
[54] P. Norby, I. G. Krogh Andersen, E. Krogh Andersen, and N. H. Andersen, J. Solid State Chem. **119**, 191 (1995).
[55] J. Fujioka, S. Ishiwata, Y. Kaneko, Y. Taguchi, and Y. Tokura, Phys. Rev. B **85**, 155141 (2012).
[56] W. C. Koehler and E. O. Wollan, J. Phys. Chem. Solids **2**, 100 (1957).
[57] S. M. Selbach, J. R. Tolchard, A. Fossdal, and T. Grande, J. Solid State Chem. **196**, 249 (2012).
[58] K. Knížek, Z. Jirák, J. Hejtmánek, M. Veverka, M. Maryško, B. C. Hauback, and H. Fjellvåg, Phys. Rev. B **73**, 214443 (2006).
[59] G. Catalan, Phase Trans. **81**, 729 (2008).

[60] J. A. Alonso, M. J. Martínez-Lope, M. T. Casais, M. A. G. Aranda, and M. T. Fernández-Díaz, J. Am. Chem. Soc. **121**, 4754 (1999).
[61] A. Hampel, P. Liu, C. Franchini, and C. Ederer, npj Quantum Mater. **4**, 5 (2019).
[62] F. Giustino, Rev. Mod. Phys. **89**, 015003 (2017).
[63] J. H. Lee, K. T. Delaney, E. Bousquet, N. A. Spaldin, and K. M. Rabe, Phys. Rev. B **88**, 174426 (2013).
[64] M. De Raychaudhury, E. Pavarini, and O. K. Andersen, Phys. Rev. Lett. **99**, 126402 (2007).
[65] M. H. Sage, G. R. Blake, C. Marquina, and T. T. M. Palstra, Phys. Rev. B **76**, 195102 (2007).
[66] A. Subedi, O. E. Peil, and A. Georges, Phys. Rev. B **91**, 075128 (2015).
[67] P. Liu, S. Khmelevskyi, B. Kim, M. Marsman, D. Li, X.-Q. Chen, D. D. Sarma, G. Kresse, and C. Franchini, Phys. Rev. B **92**, 054428 (2015).
[68] B. Kim, P. Liu, Z. Ergönenc, A. Toschi, S. Khmelevskyi, and C. Franchini, Phys. Rev. B **94**, 241113(R) (2016).
[69] J. B. Torrance, P. Lacorre, A. I. Nazzal, E. J. Ansaldo, and C. Niedermayer, Phys. Rev. B **45**, 8209 (1992).
[70] M. Ekholm, D. Gambino, H. J. M. Jönsson, F. Tasnádi, B. Alling, and I. A. Abrikosov, Phys. Rev. B **98**, 094413 (2018).